Photodecomposition of MnO_4^-: A Theoretical Study

Gennady L. Gutsev, B. K. Rao, and P. Jena

Physics Department, Virginia Commonwealth University, Richmond, Virginia 23284-2000

Received: August 2, 1999; In Final Form: September 29, 1999

The electronic and geometrical structures of the ground states and low-lying isomers of MnO_4 and MnO_4^- have been calculated as a function of spin-multiplicities by using the molecular orbital theory based on generalized gradient approximation to the density functional formalism. Total energies of isomers are used for evaluating the energetics of the MnO_4^- decay through various fragmentation channels. Two primary channels were found depending on the energy of photons. The preferred photofragmentation channel, accessible with ≈2 eV photons, is found to involve an initial excitation of the ground-state MnO_4^- anion into its peroxo isomer followed by subsequent excitations into a superoxo form. Photodetachment of an extra electron from this superoxo isomer anion leads to the formation of a neutral superoxo isomer of MnO_4, which, in turn, dissociates to $MnO_2 + O_2$. Excitations of the anion peroxo isomer into biperoxo isomer are also possible with 3.7 eV, photons and the latter could dissociate spontaneously to $MnO_2^- + O_2$. A number of other decay channels are accessible with low-energy photons, but their intensities are expected to be low because these require flipping the spin of one or more electrons.

Introduction

The permanganate anion, MnO_4^-, is a very common inorganic anion in solutions and solids and is extensively used as an oxidizing agent.[1] Its photochemical decomposition with evolution of molecular oxygen in alkaline aqueous solutions was been observed a long time ago.[2] Subsequent studies[3,4] have confirmed the evolution of O_2 during the MnO_4^- decomposition and provided order-of-magnitude estimates of its quantum yield. Using isotopic labels, Zimmerman[5] concluded that all the molecular oxygen that evolved was derived from the photodecomposition of permanganate and not from the solution. In addition, he found the quantum yield of molecular oxygen to depend strongly on the wavelength of the light, slightly on the temperature at longer wavelengths, and not at all on the composition of the solution or light intensity.

A fundamental understanding of the exact mechanism and process by which MnO_4^- photodecomposition leads to the production of O_2 has remained a difficult problem, as it involves analyzing the energetics of many possible decay channels. In Table 1 we list these channels. A thorough study of all these channels is not a trivial problem, as it involves obtaining geometries and energies of ground and excited states corresponding to isomers of the MnO_x and MnO_x^- clusters ($x \leq 4$) with different multiplicities. Kläning and Symons[6] have discussed the accessibility of several light-induced decomposition channels for MnO_4^- such as

$$MnO_4^- + h\nu \rightarrow MnO_2^- + O_2 \quad (1)$$

$$MnO_4^- + h\nu \rightarrow MnO_2 + O_2^- \quad (2)$$

$$MnO_4^- + h\nu \rightarrow MnO_3^- + O \quad (3)$$

$$MnO_4^- + h\nu \rightarrow MnO_3 + O^- \quad (4)$$

and speculated that the most probable route for oxygen formation is channel 1, in agreement with the conjecture of Zimmerman.[5] We will show later that the photofragmentation of MnO_4^- from its ground state through either channel 1 or 2 requires energies in excess of 5 eV. Thus, these direct channels cannot be accessed with visible light. Because photodecomposition occurs with visible light, one can expect additional intermediate channels to be involved in the photofragmentation process.

TABLE 1: Some Possible Channels for Photofragmentation of MnO_4^-

intermediate	final
	$MnO_2^- + O_2$, $MnO_2 + O_2^-$
$MnO_4 + e$	$MnO_4 \rightarrow MnO_{4-x} + O_x$ ($x = 1, 2, 3$)
$MnO_3^- + O$	$MnO_3^- \rightarrow MnO_{3-x} + O_x + e$ ($x = 1, 2$)
	$\rightarrow MnO_{3-x}^- + O_x$ ($x = 1, 2$)
	$\rightarrow MnO_{3-x} + O_x^-$ ($x = 1, 2$)
$MnO_3 + O^-$	$MnO_3 \rightarrow MnO_{3-x} + O_x$ ($x = 1, 2$)

Nearly three decades later, Lee et al.[7] performed a detailed study of the MnO_4^- decomposition in different solutions and discovered a long-lived (a microsecond lifetime scale) intermediate, which was conjectured to play a key role in photodecomposition of the permanganate anion. Tentatively, they attributed this intermediate to a peroxo isomer of the anion where Mn is bonded to two oxygen atoms in a molecular or associative form and the other two are in an atomic or dissociative form. Although the spectroscopy of MnO_4^- has been studied theoretically by several authors using molecular orbital calculations based on X_α, Hartree−Fock, and singles and doubles configuration interaction schemes, very little has been done for understanding the photodecomposition process of the anion from a fundamental point of view. The first step toward this understanding was undertaken recently by Nakai et al.,[8] who studied photodissociation of MnO_4^- via formation of a peroxo complex using a symmetry-adapted cluster (SAC)/SAC−configuration-interaction (SAC-CI) method. The following path was considered

$$MnO_4^- + h\nu \rightarrow [MnO_4^-(\text{peroxo})] + h\nu \rightarrow MnO_2^- + O_2 \quad (5)$$

It was concluded that this is the primary channel of the permanganate ion fragmentation. We will see below that the

10.1021/jp992731v CCC: $18.00
Published on Web 11/12/1999

energy required for the formation of a peroxo complex is 2.1 eV and the subsequent dissociation in route[5] requires 3.2 eV. However, the decomposition of MnO_4^- was observed experimentally at different photon wavelengths, namely, of 311 nm (3.99 eV) and 578 nm (2.14 eV). Note that decomposition along route[5] cannot proceed with light of 578 nm (2.14 eV) wavelength, as the second step requires 3.2 eV of energy. In addition, Nakai et al.[8] have obtained a linear geometry for MnO_2^- with their SAC/SAC-CI approach, which is in contradiction with experimental observations[9] of a bent MnO_2^- anion.

Using the density functional theory and the generalized gradient approximation (DFT-GGA) for the exchange correlation potential, we had earlier studied the energetics of neutral and anionic clusters of FeO_n ($n = 1-4$).[10,11] The DFT-GGA approach was found to be capable of reproducing the experimental values of electron affinities in the FeO_n clusters within 0.2 eV of the experiment. Similar calculations[12] using DFT-GGA technique for TiO_n and TiO_n^- ($n = 1-3$) series are also in very good agreement with the experimental data. On the contrary, the Hartree−Fock-based methods[13,14] have not done so well in treating *d* metal oxide clusters. We should also emphasize that in previous studies[10−12,15] a rather large number of isomers for both neutral and charged transition metal oxide clusters were detected. This implies that both MnO_4 and MnO_4^- should possess many isomers, and a full account of their existence and energetics is necessary in understanding the photodecomposition process.

The present work, therefore, is aimed at calculating the energetics of different decay channels of MnO_4^-, accessible with optical photons, by searching for different isomers of MnO_4 and MnO_4^-. We explore several types of MnO_4^- decay channels: (a) decomposition of MnO_4^- isomers to $MnO_2^- + O_2$ within channels conserving the ground-state multiplicity $2S + 1 = 1$; (b) paths related to initial photodetachment of the extra electron from one of the isomers of MnO_4^- followed by dissociation of the resulting neutral MnO_4 to $MnO_2 + O_2$; (c) paths involving the flipping of the spin(s) of one or more electrons at some intermediate configurations with or without detachment of the extra electron. To estimate fragmentation energies through different channels, we have to optimize the ground states of O_2, O_2^-, MnO_x, and MnO_x^- ($x = 2-4$) clusters.

In the following, we describe our theoretical approach and discuss the equilibrium geometries, electronic structure, and properties of neutral and anionic MnO_4 clusters. Finally, we propose several different fragmentation channels for MnO_4^- that are accessible with optical energies (ranging from 1.6 to 3.7 eV).

Computational Details

The calculations are performed using the molecular orbital theory where a linear combination of atomic orbitals centered at various atomic sites constitutes the cluster wave function. The many-electron potential is constructed by using the DFT-GGA for the exchange correlation functional. We have used Becke's exchange[16] and Perdew−Wangs' correlation[17] functionals, referred to as BPW91, in the Gaussian94 software.[18] For the atomic orbitals we have used the standard 6-311+G* basis [Fe: (10s7p4d1f); O: (5s4p1d)]. These choices are known to yield results in very good agreement with several experiments.[10,11,19,20]

Geometry optimizations of clusters were carried out by examining the gradient forces at each atomic site and moving the atoms along the path of steepest descent until the forces vanish with respect to a threshold value of 3×10^{-4}. Subsequent harmonic frequency calculations were performed to confirm that optimized geometries correspond to stationary states. To estimate the thermodynamic stability of manganese oxide clusters, we have evaluated their fragmentation channels with evolution of O and O_2 (for MnO_4) as well as O^- and O_2^- (for MnO_4^-). These fragmentation energies correspond to the differences in total energies of fragments F_i formed in a particular decay channel and the total energy of an initial compound M, namely

$$D_e(\mathrm{M}) = \sum_i E_{tot}(F_i) - E_{tot}(\mathrm{M}) \qquad (6)$$

The calculations were carried out for different spin multiplicities and possible isomers MnO_4^- and MnO_4 could have.

It should be pointed out that, originally, Kohn and Sham[21] formulated the DFT for the ground states only. It was proven later[22,23] that the DFT can be extended also for the lowest energy states in each particular symmetry (spatial and spin) channel. This is important because isomers of a ground-state polyatomic system may have higher energies and thus could be considered as excited states for which the DFT should not be valid. However, isomers with geometries different from the ground-state geometry possess different spatial symmetries, and should be attributed to different electronic−nuclear symmetry channels even if the corresponding electronic configurations have the same symmetry labels (e. g., $^1A_1$ within T_d, C_{2v}, or D_{2d} point-symmetry groups).

Results and Discussion

A. Geometry Optimizations. We first discuss the geometries of MnO_4 and MnO_4^-. Because they have odd and even numbers of electrons respectively, the geometries need to be optimized for spin multiplicities of $M = 2S + 1 = 2, 4, 6, \ldots$ for MnO_4 and $M = 1, 3, 5, \ldots$ for MnO_4^-. In addition, all the oxygen atoms can bind dissociatively (atomic form), associatively (molecular form), or in a mixed form (two dissociated and two associated). In the latter, the orientation of the molecular oxygen bond can also be different. Depending on their orientation, the isomer is either labeled peroxo or superoxo.

We have performed an exhaustive search for the geometries for the above spin multiplicities and oxygen configurations. The results of optimizations are presented in Figures 1 and 2 for MnO_4 and MnO_4^-, respectively. We label the isomers in Figure 1 from n1 to n10 where n refers to the neutral (there are nine isomers within 2.8 eV from the ground state). Similarly for the anion isomers in Figure 2, we choose to label them from a1 to a10 where a refers to anions (there are nine isomers within 5.8 eV from the ground state). Harmonic vibrational frequencies of the isomers are given in the corresponding figure captions. All these frequencies are real, which indicates that all clusters correspond to stationary states. Relative energies of both neutral and anionic isomers are given in Table 2 with respect to the total energy of the ground state of MnO_4.

The ground state of MnO_4 was found to have C_{2v} symmetry representing a distorted tetrahedron with atomically bonded oxygens and $^2B_2$ electronic configuration (see Figure 1, n1). No experimental or theoretical data are available on the structure of neutral MnO_4 clusters, to the best of our knowledge. To check if there are additional C_{2v} configurations of MnO_4 with dissociated oxygens, we have optimized geometries for wave functions transforming according to other irreducible representations (A_1, B_1, and A_2) of C_{2v} point-symmetry group. The geometry and the total energy of the $^2B_1$ state converged to those of the $^2B_2$ state; that is, these two states are degenerate in

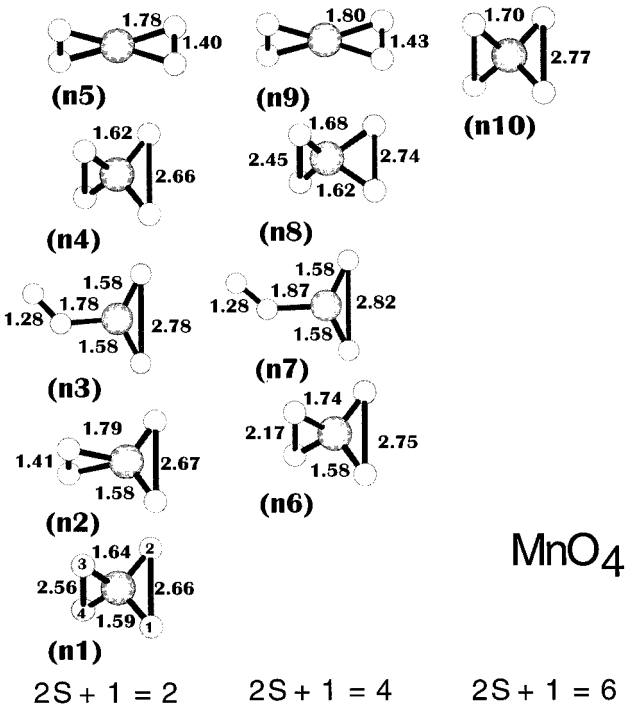

Figure 1. Optimized geometrical configurations of MnO_4 in the ground state (the reference state) and its isomers with multiplicities $2S + 1 = 2$, 4, and 6. Harmonic vibrational frequencies (in cm^{-1}) are as follows: n1: $a_1 = 263, 390, 829, 925$; $b_1 = 343, 867$; $a_2 = 285$; $b_2 = 350, 551$. n2: $a_1 = 337, 577, 960, 1007$; $b_1 = 223, 614$; $a_2 = 230$; $b_2 = 254, 1030$. n3: $a' = 106, 148, 202, 283, 308, 475, 962$ 1038, 1245; n4: $a_1 = 311, 360, 806, 850$; $a_2 = 345$; $e(b_1,b_2) = 426, 1760$. n5: $a_1 = 504, 682, 1001, 1009$; $a_2 = 358$; $e(b_1,b_2) = 129, 541$. n6: $a_1 = 249, 347, 743, 938$; $b_1 = 222, 641$; $a_2 = 238$; $b_2 = 275, 971$. n7: $a' = 134, 243, 298, 496, 866, 914, 1081$; $a'' = 107, 241$. n8: $a_1 = 198, 230, 677, 836$; $b_1 = 278, 628$; $a_2 = 238$; $b_2 = 229, 657$. n9: $a_1 = 477, 674, 945, 971$; $a_2 = 148$; $e(b_1,b_2) = 107, 486$. n10: $a_1 = 66, 134, 579, 771$; $b_1 = 68, 568$; $a_2 = 133$; $b_2 = 94, 585$. (near T_d symmetry).

total energy and correspond to mirror-reflected geometrical configurations in a fixed coordinate frame.

We also found an isomer of neutral MnO_4 with all four oxygens bound dissociatively within D_{2d} symmetry. This isomer, given in Figure 1 (n4), lies 1.4 eV above the ground state and has $^2A_1$ electronic state. An $^2A_2$ state with D_{2d} symmetry was found to be above $^2B_1$ and $^2B_2$ states by 0.04 eV only, but this state has a doubly degenerate imaginary e frequency of 979*i* (e $\rightarrow$ b_1, b_2 upon reducing $D_{2d} \rightarrow C_{2v}$) and represents a double saddle point on the potential energy surface.

Similar to that of FeO_4,[10,24] MnO_4 has a peroxo isomer where two oxygen atoms are bound to Mn dissociatively, whereas the other two are bound associatively (n2, see Figure 1). Note that the distance between peroxo oxygens is 1.41 Å, which can be compared with the bond lengths of 1.21 Å in the $^3\Sigma^-_g$ ground state of O_2[25], 1.23 Å in the excited $^1\Delta_g$ state of O_2[26], and 1.36 Å in the $^2\Pi_g$ ground state of O_2^-.[27] The peroxo isomer is above the ground state of neutral MnO_4 by 0.2 eV. Approximately the same upward shift in total energy was found for a peroxo isomer of FeO_4 with respect to its D_{2d} ground state[10] as well. The superoxo isomer of MnO_4 (n3 in Figure 1) is flat and is above the ground state by 1 eV.

To have a qualitative understanding of why the ground state of MnO_4 and its peroxo isomer are energetically close, we consider the results of the natural bond analysis (NBO),[28] which is based on the use of localized orbitals constructed from the occupancy-weighted symmetric orthogonalized natural atomic orbitals and provides effective electronic configurations for each

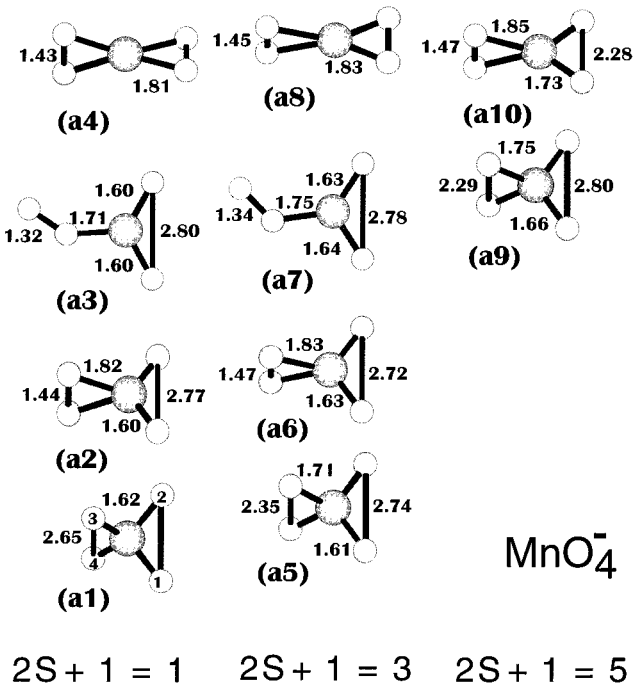

Figure 2. Optimized geometrical configurations of MnO_4^- in the ground state (the reference energy is the total energy of the ground state of MnO_4) and its isomers with multiplicities $2S + 1 = 1$, 3, and 5. Harmonic vibrational frequencies (in cm^{-1}) are as follows: a1: $e = 352$; $t_2 = 400, 932$; $a_1 = 873$. a2: $a_1 = 320, 605, 914, 943$; $b_1 = 248, 494$; $a_2 = 287$; $b_2 = 257, 972$. a3: $a' = 125, 132, 256, 303, 345, 571, 924, 977, 1160$. a4: $a_1 = 515, 701, 934, 937$; $a_2 = 317$; $e(b_1,b_2) = 131, 467$. a5: $a_1 = 253, 356, 909, 945$; $b_1 = 330, 945$; $a_2 = 269$; $b_2 = 304, 679$. a6: $a_1 = 327, 562, 874, 925$; $b_1 = 189, 500$; $a_2 = 165$; $b_2 = 207, 892$. a7: $a' = 107, 137, 241, 243, 298, 496, 866, 913, 1081$. a8: $a_1 = 486, 646, 888.$ 900; $a_2 = 101$; $e(b_1,b_2) = 125, 413$. a9: $a_1 = 157, 312, 697, 798$; $b_1 = 152, 601$; $a_2 = 189$; $b_2 = 115, 632$. a10: $a_1 = 296, 525, 817, 882$; $b_1 = 139, 436$; $a_2 = 144$; $b_2 = 112, 549$.

TABLE 2: Energies (in eV) of Different Isomers of MnO_4 and MnO_4^- Relative to Total Energy of Ground State of MnO_4 (−1452.02491 hartree) as well as Their Corresponding Symmetries and Electronic States

MnO_4			MnO_4^-		
figure 1	symmetry	ΔE_{tot}	figure 2	symmetry	ΔE_{tot}
n1	C_{2v}, $^2B_2$	0.0	a1	T_d, $^1A_1$	−5.0[a]
n2	C_{2v}, $^2A_1$	0.2	a2	C_{2v}, $^1A_1$	−2.9
n3	C_s, $^2A'$	1.0	a3	C_s, $^1A'$	−1.9
n4	D_{2d}, $^2A_1$	1.4	a4	D_{2d}, $^1A_1$	+0.8
n5	D_{2d}, $^2A_1$	2.8			
n6	C_{2v}, $^4B_2$	1.4	a5	C_{2v}, $^3B_2$	−3.4
n7	C_s, $^4A''$	1.6	a6	C_{2v}, $^3A_2$	−2.6
n8	C_{2v}, $^4A_2$	1.6	a7	C_s, $^3A''$	−1.8
n9	D_{2d}, $^4A_2$	2.3	a8	D_{2d}, $^3A_2$	+0.5
n10	C_{2v}, $^6A_2$	2.8	a9	C_{2v}, $^5B_2$	−1.7
			a10	C_{2v}, $^5B_1$	−0.7

[a] Experimental estimate of 4.8 eV[19] for the adiabatic electron affinity of MnO_4 agrees well with our calculated value of 5.0 eV.

atom in a cluster. In the $^2B_2$ ground state of MnO_4 (n1 in Figure 1), effective atomic configurations are: Mn ($4s^{0.24}3d^{5.76}$), $O_{1,2}$ ($2s^{1.92}2p^{4.29}$), and $O_{3,4}$ ($2s^{1.91}2p^{4.34}$), whereas in peroxo isomer (n2 in Figure 1) the atomic populations are: Mn ($4s^{0.23}3d^{5.59}$), $O_{1,2}$ ($2s^{1.92}2p^{4.43}$), (the shorter bonds), and $O_{3,4}$ ($2s^{1.86}2p^{4.34}$) (the longer bonds). One can see a somewhat larger participation of 2s electrons in peroxo O−O bonding. It is also interesting to compare partial populations of the Mn 3d manifold in both cases. In the ground state, they are determined by the atomic configuration: $3d_{xy}^{1.19}3d_{xz}^{1.15}3d_{yz}^{1.12}3d_{x^2-y^2}^{1.13}3d_{z^2}^{1.18}$, whereas the per-

TABLE 3: Fragmentation Energies [(D_e), in eV] of MnO_4 and MnO_4^-, Computed According to eq 6[a]

MnO_4		MnO_4^-	
channel	D_e	channel	D_e
$MnO_4 \rightarrow MnO_2 + O_2$	2.28	$MnO_4^- \rightarrow MnO_4 + e$	4.96
$\rightarrow MnO_3 + O$	3.18	$\rightarrow MnO_3^- + O$	4.99
		$\rightarrow MnO_2^- + O_2$	5.30
		$\rightarrow MnO_3 + O^-$	6.56
		$\rightarrow MnO_2 + O_2^-$	6.86

[a] Our computed D_es of O_2 and O_2^- are 5.83 and 4.64, respectively. Experimental values are 5.12 and 4.1 eV for O_2 and O_2^-, respectively.[25]

oxo isomer has $3d_{xy}^{1.16}3d_{xz}^{1.11}3d_{yz}^{1.07}3d_{x^2-y^2}^{1.12}3d_{z^2}^{1.13}$. As one can see, there are no "preferable" d orbitals, which can be responsible for the interaction with the peroxo oxygens. Hence, some decrease in participation of the Mn d manifold in bonding in this isomer has to be considered as compensated by stronger peroxo O−O bonding.

Quartet states of MnO_4 (n6−n9 in Figure 1) are well above the ground state, and the first sextet state (n10) is above the dissociation limit $MnO_4 \rightarrow MnO_2 + O_2$ (see Table 3). The doublet (D_{2d}, $^2A_1$) state is also above this dissociation limit, but the reasons for the (meta)stability of the latter and the former states appear to be different. In the case of the sextet state, there are steric obstacles toward decreasing the bond length of an oxygen−oxygen pair (to bring it to a peroxo type), whereas the doublet state is stable toward dissociation to MnO_2 (peroxo) + O_2. This is because the lowest energy peroxo isomer of MnO_2 is above the ground state of MnO_2 by about 3 eV.[29]

The geometry of the ground state of MnO_4^- was found to have T_d symmetry (see Figure 2, a1) with the $^1A_1$ electronic state, in agreement with experiment.[1] Our calculated Mn−O bond length of 1.620 Å and vibrational frequencies $\omega(e) = 352$, $\omega(t_2) = 400$, 932, and $\omega(a_1) = 873$ cm^{-1} are in good agreement with the experimental bond length of 1.629 ± 0.008 Å[30] and frequencies of $\omega(e) = 348$, $\omega(t_2) = 390$, 910, and $\omega(a_1) = 838$ cm^{-1},[31] respectively, obtained in salts. The peroxo (C_{2v},$^1A_1$) isomer of the anion is above the ground state of MnO_4^- by 2.1 eV, in contrast to the neutral case in which the corresponding energy difference is only 0.2 eV. Such a big difference in energy gaps between the ground states of MnO_4 and MnO_4^- and their peroxo isomers can be related to the spatial distribution of the extra electron in anion isomers. In the ground state of MnO_4^-, the extra electron is delocalized over four oxygen atoms that are equivalent by symmetry, and each oxygen atom has an electron affinity of 1.46 eV.[32] Because the peroxo isomer contains a "clamped" oxygen pair with relatively low electron affinity (0.451 ± 0.007 eV[33]), the energy gain in attaching an electron to the peroxo form is much smaller. According to the NBO analysis, the effective atomic configurations in the ground state of MnO_4^- are: Mn ($4s^{0.23}3d^{5.75}$) and O ($2s^{1.91}2p^{4.58}$), whereas in the peroxo isomer they are: Mn ($4s^{0.31}3d^{5.75}$), $O_{1,2(diss)}$ ($2s^{1.91}2p^{4.66}$), and $O_{3,4(peroxo)}$ ($2s^{1.86}2p^{4.49}$). Thus, this analysis confirms that the extra electron is localized mainly over two dissociatively bound oxygen atoms of the isomer, and the electron affinity of the peroxo isomer (2.9 eV) is larger than the electron affinity of MnO_2 (2.0 eV) by only 0.9 eV, and is even somewhat smaller than the electron affinity of MnO_3, 3.2 eV.[34]

Next we consider the population of Mn 3d orbitals in these two configurations of MnO_4^-. In the ground-state configuration (a1, Figure 1) they are $3d_{xy}^{1.13}3d_{xz}^{1.13}3d_{yz}^{1.13}3d_{x^2-y^2}^{1.18}3d_{z^2}^{1.18}$ and in the peroxo isomer (a2, Figure 1) they are $3d_{xy}^{0.96}3d_{xz}^{0.91}3d_{yz}^{0.99}3d_{x^2-y^2}^{1.49}3d_{z^2}^{1.41}$. One can see that the isomer possesses a well-expressed disparity between occupations of $3d_{x^2-y^2}$ and d_{z^2} orbitals of the central atom (e components in T_d symmetry) and 3d atomic orbitals arising from the t_1 manifold. That is, the extra electron is localized in the isomer (note that the peroxo group rests inside the *yz* plane). As follows from Table 2, the MnO_4^- anion has at least eight isomers (two singlets, three triplets, and two septets) that are stable toward autodetachment of an extra electron.

B. Electron Affinity of MnO_4. The uniqueness of MnO_4^- is that it is one of the most stable anions in the transition metal oxide cluster series. This is due to the anomalously large amount of energy MnO_4 gains after the attachment of an extra electron. The electron affinity of MnO_4, which measures the energy difference between the ground states of the anion and the neutral, is found to be rather large (about 5 eV; see Table 2) and agrees well with the experimental value of 4.80 eV.[19] This value exceeds the electron affinity of Cl (3.62 eV[32]), the largest electron affinity among all atoms in the periodic table, which puts MnO_4 into the class of superhalogens[35−37] with the general formula of MO_n where the coordination number *n* fulfills the requirement $2n = k + 1$. Here *k* is the maximal formal valence of the central atom. This requirement is fulfilled in MnO_4, since $n = 4$ and $k = 7$, and the extra electron fills the lowest unoccupied molecular orbital. This does not contain contributions from the central atom by symmetry, as the anion has a tetrahedral ground-state geometry. The resulting MnO_4^- anion has a closed-shell structure and is thermodynamically and electronically very stable.

C. Electronic Absorption Spectra. Experimental electronic absorption spectra[38,39] of MnO_4^- have been the subject of numerous theoretical studies in which excitation energies were estimated in terms of orbital-to-orbital vertical transitions.[40−43] Principal features of experimental spectra were summarized by Dickson and Ziegler[42] and we give here only a brief summary. Electronic spectra of MnO_4^- have: (a) a weak band near 1.75 eV; (b) a strong band at 2.25 eV; (c) strong superimposed bands at 3.10 and 3.75 eV; and (d) strong featureless superimposed bands starting at about 4.7 eV and having maxima at 5.3 and 5.8 eV. To see if these features are consistent with the energetics of different isomers of MnO_4^-, we use the results in Table 2. Adiabatic energies of the low-energy excitations [i.e., differences between total energies of the MnO_4^- ground state and its lowest triplet and singlet states (a5 and a2 in Figure 2)] are 1.6 and 2.1 eV, respectively, which are in good agreement with experimental values of 1.75 and 2.25 eV, respectively. The bands near 3 eV could be tentatively related to excitations leading to formation of superoxo isomers of MnO_4^-. The bands above 4.8 eV (i.e., above the extra electron autodetachment threshold) could be related with the formation of metastable anion states, such as (D_{2d}, $^1A_1$) and (D_{2d}, $^3A_2$) embedded in the photodetachment continuum. Thus, one can assign the optical excitations near 2 eV to the formation of peroxo and near 3 eV to the formation of superoxo isomers of MnO_4^-. Excitations above 4.8 eV lead to the photodetachment of an extra electron (and the formation of a neutral isomer). It can also result in the formation of a metastable anion state, which can then dissociate into fragment anions or autodetach an extra electron.

D. Photofragmentation Patterns. The fragmentation of MnO_4^- leading to the evolution of O_2, as mentioned earlier, can proceed in a number of ways. The only process that does not require any intermediate step involves dissociation of $MnO_4^- \rightarrow MnO_2^- + O_2$. All other processes require intermediate steps. For example, MnO_4^- can first autodetach an electron and then dissociate, namely

$$MnO_4^- + h\nu \rightarrow MnO_4 + e \rightarrow MnO_2 + O_2 \qquad (7)$$

Similarly, MnO_4^- can also fragment to MnO_3 or MnO_3^-, which can then further dissociate to yield molecular oxygen. Thus, calculations of the energies needed for the various dissociative channels require the knowledge of the ground-state energies of MnO_x and MnO_x^- (≤ 3). We have obtained these values by optimizing their ground-state geometries. A detailed account on the structure of these clusters, together with experimental photodetachment spectra, will be presented elsewhere.[34]

Here, we only present the fragmentation energies calculated using eq 6. Some of these results are given in Table 3. Note that the dissociation of MnO_4^- that could yield O_2 directly or through any intermediate steps would require energies in excess of 5 eV. This is clearly beyond the visible range. The fact that light of wavelengths of 311 nm (3.99 eV) and 578 nm (2.14 eV) can photodecompose MnO_4^- suggests that the anion must be excited to higher isomers before fragmentation. This is where a detailed understanding of the energies of different isomers of MnO_4^- and MnO_4 is useful. From the data presented in Table 3 and Figures 1 and 2, we can construct all possible channels of fragmentation that are accessible with visible light.

We outline 10 such channels, from which six channels require energies of less than 3.5 eV and yield $MnO_2 + O_2$ after photodetachment of the extra electron from the permanganate anion. Four other channels require energies of less than 3.8 eV and yield $MnO_2^- + O_2$. Each of these channels proceeds in multiple steps in which the MnO_4^- anion is first excited to a higher energy isomer before fragmentation. We first discuss the channels leading to decomposition of MnO_4^- to $MnO_2 + O_2$. These are listed in Scheme 1. Note that in the above, e↑ indicates the electron photodetachment, and S−T indicates a singlet−triplet electronic excitation.

In channel I, the ground state of MnO_4^- (a1 in Figure 2) is excited to its peroxo isomer (a2 in Figure 2) with an energy of 2.1 eV. With a further excitation of 1.0 eV, the peroxo anion converts into a superoxo anion (a3 in Figure 2). At this stage, the superoxo anion autodetaches its extra electron with the help of a photon of energy 1.9 eV. The resulting superoxo neutral MnO_4 (n7 in Figure 1), then, needs 0.7 eV to dissociate to $MnO_2 + O_2$. Thus, the entire photodecomposition in channel I can happen with photon energies of less than 2.1 eV. This, we believe, is the most preferable channel.

In channels II and III, although the photodecomposition can take place with energies less than 2.1 eV, it involves transitions from a singlet anion (a2 in Figure 2) to triplet anions (a6 or a7 in Figure 2), respectively. Because this will require additional processes for conserving the total momentum, we expect these channels to be less preferred. More preferable than channels II and III will be channels IV and V, even though the latter require higher energy photons, as they do not involve any spin-flip process.

Other channels that compete with channels I, IV, and V are channels involving the dissociation $MnO_4^- \rightarrow MnO_2^- + O_2$. In Scheme 2, we list these channels: Here T-Qn indicates a triplet−quintet excitation. The most favored channel in this process is channel VII. The MnO_4^- anion (a1 in Figure 2) is first excited to its peroxo isomer (a2 in Figure 2) and then to a state where the oxygen atoms bind molecularly (biperoxo isomer a4 in Figure 2). This requires photons of 3.7 eV energy. The resulting isomer is above the dissociation threshold of $MnO_2^- + O_2$. The a4 decay process is exothermic and releases an energy of 0.5 eV as the photodecomposition proceeds. Channel VIII, although requiring photons of the least energy ($\leq$1.6 eV), is highly unlikely, as it involves two spin-flips when going from a1 to a5 and a7 to a10 in Figure 2.

SCHEME 1

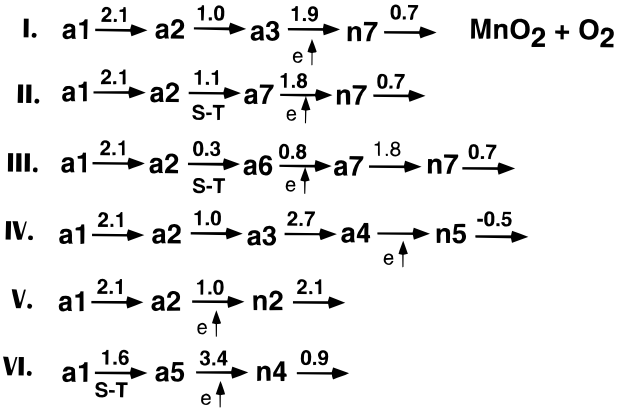

SCHEME 2

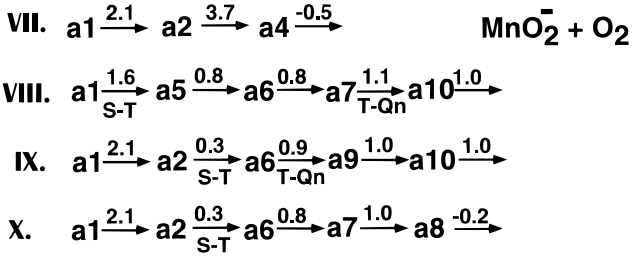

We should emphasize that our analysis of the photodecomposition channels of MnO_4^- is based solely on the energies of the products. For a more detailed description, one needs to address such complicated questions as the barrier heights toward transformations of isomers into each other, lifetimes of isomers, transition probabilities given at the first order by Franck−Condon factors, and vibrational excitation−deexcitation processes. A detailed consideration of such subtle questions would require the use of advanced quantum dynamic time-dependent methods and is out of the scope of the present work on the basis of the Born−Oppenheimer (BO) approximation. However, we believe that the main features in photofragmentation patterns of the MnO_4^- could be described within the BO approximation, and stationary states obtained for MnO_4 and MnO_4^- would be a useful guide for more quantitative studies.

Conclusion

Using the DFT-GGA corrections we have obtained the ground states of MnO_4 and MnO_4^- and nine other isomers each of these species corresponding to different spin multiplicities. Total energies of isomers are used in evaluating the energetics of the MnO_4^- decay through various fragmentation channels. The anion is thermodynamically more stable than its neutral parent, MnO_4, and possesses at least eight isomers stable toward autodetachment of the extra electron.

We have identified 10 possible channels requiring photon energies of less than 3.8 eV by which MnO_4^- can photofragment to produce molecular oxygen. All channels require the anion to be excited before fragmentation if the photon energies lie in the optical range. Among these, two channels are considered to be preferable. The one requiring energies of less than 2.2 eV involves the excitation of the permanganate anion to its peroxo isomer, which is further excited to its superoxo isomer form. At this stage, the electron is detached, leaving the neutral in its

superoxo isomer of MnO_4. An energy of only 0.7 eV is needed for this isomer to dissociate to $MnO_2 + O_2$. The second channel requires energies of up to 3.7 eV but fewer steps. As in the above channel, the MnO_4^- anion is first excited to its peroxo form, which then can be excited to its biperoxo form (that contains two molecular oxygen pairs bound to Mn). This form dissociates spontaneously to $MnO_2^- + O_2$ as it lies above the dissociation threshold. The other eight channels either require higher energies, larger number of intermediate steps, or spin-flips during the photodecomposition process and are thus considered less likely.

It may be possible to photodecompose MnO_4^- more easily by using polarized light, which can couple to the spin-flip transition in isomers during the decomposition process. Such experimental studies are encouraged. We should emphasize that the analysis presented here does not take into account other issues such as energy barriers and lifetimes that may be relevant for a quantitative calculation of the quantum yield. Nevertheless, this analysis is by far the most exhaustive study of the photodecomposition of MnO_4^- from a theoretical point of view performed thus far.

Acknowledgment. This work was supported in part by a grant to Virginia Commonwealth University by the Department of Energy (grant no. DE-FG05-87ER61316). We thank Dr. V. G. Zakrzewski for help in a more effective use of GAUSSIAN94.

References and Notes

(1) Cotton, F. A.; Wilkinson G. *Advanced Inorganic Chemistry*; Wiley-Interscience: New York, 1988.
(2) Mathews, J. H.; Dewey, L. H. *J. Phys. Chem.* **1913**, *17*, 211.
(3) Rideal, E. K.; Norrish, R. G. W. *Proc. R. Soc. London* **1923**, *A103*, 342.
(4) Rao, A. L. S. *Proc. Indian Acad. Sci.* **1937**, *6A*, 293.
(5) Zimmerman, G. *J. Chem. Phys.* **1955**, *23*, 825.
(6) Kläning, U.; Symons, M. C. R. *J. Chem. Soc.* **1959**, 3269.
(7) Lee, D. G.; Moylan, C. R.; Hayashi, T.; Brauman, J. I. *J. Am. Chem. Soc.* **1987**, *109*, 3003.
(8) Nakai, H.; Ohmori, Y.; Nakatsuji, H. *J. Phys. Chem.* **1995**, *99*, 8550.
(9) Chertihin, G. V.; Andrews, L. *J. Phys. Chem.* **1997**, *101*, 8547.
(10) Gutsev, G. L.; Khanna, S. N.; Rao, B. K.; Jena, P. *Phys. Rev. A* **1999**, *59*, 3681.
(11) Gutsev, G. L.; Khanna, S. N.; Rao, B. K.; Jena, P. *J. Phys. Chem. A* **1999**, *103*, 5812.
(12) Walsch, M. B., King, R. A., and Schaefer, H. F. III. *J. Chem. Phys.* **1999**, *110*, 5224.
(13) Johansen, H. *Mol. Phys.* **1983**, *49*, 1209.
(14) Buijse, M. A.; Baerends, E. J. *J. Chem. Phys.* **1990**, *93*, 4129.
(15) Veliah, S.; Xiang, K. H.; Pandey, R.; Recio, J. M.; Newsam, J. M. *J. Phys. Chem.* **1998**, *102*, 1126.
(16) Becke, A. D. *Phys. Rev. A* **1988**, *38*, 3098.
(17) Perdew, J. P.; Wang, Y. *Phys. Rev. B* **1991**, *45*, 13244.
(18) *Gaussian 94, Revision B.1*; Frisch, M. J.; Trucks, G. W.; Schlegel, H. B.; Gill, P. M. W.; Johnson, B. G.; Robb, M. A.; Cheeseman, J. R.; Keith, T.; Petersson, G. A.; Montgomery, J. A.; Raghavachari, K.; Al-Laham, M. A.; Zakrzewski, V. G.; Ortiz, J. V.; Foresman, J. B.; Cioslowski, J.; Stefanov, B. B.; Nanayakkara, A.; Challacombe, M.; Peng, C. Y.; Ayala, P. Y.; Chen, W.; Wong, M. W.; Andres, J. L.; Replogle, E. S.; Gomperts, R.; Martin, R. L.; Fox, D. J.; Binkley, J. S.; Defrees, D. J.; Baker, J.; Stewart, J. P.; Head-Gordon, M.; Gonzalez, C.; Pople, J. A. Gaussian, Inc., Pittsburgh, PA, 1995.
(19) Gutsev, G. L.; Rao, B. K.; Jena, P., Wang, X. B.; Wang, L. S. *Chem Phys. Lett.* in press.
(20) Gutsev, G. L.; Reddy, B. V.; Khanna, S. N.; Rao, B. K.; Jena, J. *Phys. Rev. B* **1998**, *58*, 14131.
(21) Kohn, W.; Sham, L. J. *Phys. Rev.* **1965**, *140*, A1133.
(22) Gunnarsson, O.; Lundqvist, B. I. *J. Chem. Phys.* **1976**, *13*, 4274.
(23) Gross, E. K. U.; Oliveira, L. N.; Kohn, W. *Phys. Rev. A* **1988**, *37*, 2809.
(24) Chertihin, G. V.; Saffel, W.; Yustein, J. T.; Andrews, A.; Neurock, M.; Ricca, A.; Bauschlicher, C. W. Jr. *J. Phys. Chem.* **1996**, *100*, 5261.
(25) Huber, K. P.; Herzberg, G. *Constants of Diatomic Molecules*; Van Nostrand-Reinhold: New York, 1979.
(26) Vincent, M. A.; Hillier, I. H. *J. Phys. Chem.* **1995**, *99*, 3109.
(27) Parlant, G.; Fiquet-Fayard, F. *J. Phys. B* **1976**, *9*, 1617.
(28) Reed, A. E.; Curtiss, L. A.; Weinhold, F. *Chem. Rev.* **1988**, *88*, 899.
(29) Gutsev, G. L.; Rao, B. K., Jena, P. *J. Phys. Chem.*, to be submitted.
(30) Palenik, G. *Inorg. Chem.* **1967**, *6*, 503.
(31) Homborg, H. *Z. Anorg. Allg. Chem.* **1983**, *498*, 25.
(32) Hotop, H.; Lineberger, W. C. *J. Phys. Chem. Ref. Data* **1985**, *14*, 731.
(33) Travers, M. J.; Cowles, D. C.; Ellison, G. B. *Chem. Phys. Lett.* **1989**, *164*, 449.
(34) Gutsev, G. L.; Rao, B. K.; Jena, P.; Li, X.; Wang, L. S., to be submitted.
(35) Gutsev, G. L.; Boldyrev, A. I. *Chem. Phys.* **1981**, *56*, 277.
(36) Gutsev, G. L.; Boldyrev, A. I. *Chem. Phys. Lett.* **1984**, *108*, 255.
(37) Gutsev, G. L.; Boldyrev, A. I. *Adv. Chem. Phys.* **1985**, *61*, 169.
(38) Müller, A.; Diemann, E. *Chem. Phys. Lett.* **1971**, *9*, 369.
(39) Johnson, L. W.; McGlynn, S. P. *Chem. Phys. Lett.* **1971**, *10*, 595.
(40) Ziegler, T.; Rauk, A.; Baerends, E. J. *Chem. Phys.* **1976**, *16*, 209.
(41) Gutsev, G. L.; Levin, A. A. *Struct. Chem. (Russian Transl.)* **1979**, *19*, 838.
(42) Dickson, R. M.; Ziegler, T. *Int. J. Quantum Chem.* **1996**, *58*, 681.
(43) Stücl, A. C.; Daul, C. A.; Güdel, H. U. *Int. J. Quantum Chem.* **1997**, *61*, 579.